Molecular Psychiatry
https://doi.org/10.1038/s41380-019-0485-2

ARTICLE

Structural interaction between DISC1 and ATF4 underlying transcriptional and synaptic dysregulation in an iPSC model of mental disorders

Xinyuan Wang[1,2] · Fei Ye[3,4] · Zhexing Wen[5,6] · Ziyuan Guo[2] · Chuan Yu[3] · Wei-Kai Huang[2,7] · Francisca Rojas Ringeling[8] · Yijing Su[2] · Wei Zheng[9] · Guomin Zhou[1] · Kimberly M. Christian[2] · Hongjun Song[2,10,11,12] · Mingjie Zhang[3,4] · Guo-li Ming[2,10,11,13]

Received: 13 October 2018 / Revised: 1 April 2019 / Accepted: 17 May 2019

Abstract

Psychiatric disorders are a collection of heterogeneous mental disorders arising from a contribution of genetic and environmental insults, many of which molecularly converge on transcriptional dysregulation, resulting in altered synaptic functions. The underlying mechanisms linking the genetic lesion and functional phenotypes remain largely unknown. Patient iPSC-derived neurons with a rare frameshift *DISC1* (Disrupted-in-schizophrenia 1) mutation have previously been shown to exhibit aberrant gene expression and deficits in synaptic functions. How DISC1 regulates gene expression is largely unknown. Here we show that Activating Transcription Factor 4 (ATF4), a DISC1 binding partner, is more abundant in the nucleus of *DISC1* mutant human neurons and exhibits enhanced binding to a collection of dysregulated genes. Functionally, overexpressing ATF4 in control neurons recapitulates deficits seen in *DISC1* mutant neurons, whereas transcriptional and synaptic deficits are rescued in *DISC1* mutant neurons with CRISPR-mediated heterozygous *ATF4* knockout. By solving the high-resolution atomic structure of the DISC1–ATF4 complex, we show that mechanistically, the mutation of DISC1 disrupts normal DISC1–ATF4 interaction, and results in excessive ATF4 binding to DNA targets and deregulated gene expression. Together, our study identifies the molecular and structural basis of an DISC1–ATF4 interaction underlying transcriptional and synaptic dysregulation in an iPSC model of mental disorders.

Introduction

Many major mental disorders, including schizophrenia, are neurodevelopmental disorders resulting from genetic interruption and synaptic dysfunction [1–3]. With the rapid progress in identifying genetic variants conferring risk for psychiatric disorders, it has become evident that the genetics of most psychiatric disorders are complex due to the co-occurrence of multiple susceptibility variants with low penetrance, which in turn contribute to highly variable clinical phenotypes [4]. A major missing link that remains to be addressed is how genetic lesions modulate molecular networks to affect neuronal function. Patient-derived induced pluripotent stem cells (iPSCs) have a unique advantage as a model system to address this question as these iPSCs maintain the genetic predisposition of patients and can be differentiated into relevant human neural cell types; and rare, but highly penetrate genetic risk factors provide an unique entry point for mechanistic analysis [5, 6].

Disrupted-in-schizophrenia 1 (*DISC1*), a genetic risk factor implicated in multiple psychiatric [7, 8] and neurological disorders [9, 10], has been shown to regulate key aspects of neural development, ranging from proliferation

These authors contributed equally: Xinyuan Wang, Fei Ye

Supplementary information The online version of this article (https://doi.org/10.1038/s41380-019-0485-2) contains supplementary material, which is available to authorized users.

✉ Hongjun Song
shongjun@pennmedicine.upenn.edu

✉ Mingjie Zhang
mzhang@ust.hk

✉ Guo-li Ming
gming@pennmedicine.upenn.edu

Extended author information available on the last page of the article.

Published online: 23 August 2019

and differentiation of neural progenitors, neuronal morphological development, to synaptic development and function [11–17]. DISC1 protein has an unusually large interactome with over a hundred binding partners and is hypothesized to function as a major hub protein for signal integration of neurodevelopmental and disease-related pathways in a cell type and context-dependent manner [18–21]. For example, DISC1 regulates cell division, metabolism, and synaptic function based on its localization and protein interaction in cytoplasmic compartments, such as kinetochore, mitochondria, and pre- and post-synaptic sites, respectively [8, 15, 22, 23]. The majority of interactions identified in the interactome, however, have yet to be validated and the functional outcome of such interactions remains to be determined.

Activating Transcription Factor 4 (ATF4), also known as CREB-2, belongs to the ATF/CREB transcription factor family proteins and has been shown to play an important role in synaptic plasticity, memory suppression or memory improvement in various animal models [24–26]. A recent study identified *ATF4* as one of the 709 genes that are significantly associated with general cognitive function in a gene-based association study [27]. Interestingly, ATF4 was initially identified as a member of the DISC1 interactome via a yeast two-hybrid screen and later studies suggested that ATF4 and DISC1 form a transcriptional repression complex and regulate gene expression in the nucleus [28–31]. When overexpressed in heterologous cell lines, disease-relevant nonsynonymous DISC1 variants were shown to affect ATF4 nuclear targeting [32]. We have previously reported that cortical neurons derived from patient iPSCs (schizophrenia or major depression) harboring a rare 4 base-pair frameshift mutation in the *DISC1* locus exhibit dysregulated expression of a large set of genes encoding synapse-related proteins [33]. Whether DISC1 and ATF4 also interact in human neurons to regulate gene expression and contribute to disease relevant cellular phenotypes is completely unknown.

In the present study, we examined the relationship between a *DISC1* gene mutation and ATF4 by assessing the transcriptional and functional consequences of *ATF4* manipulations in *DISC1* mutant and control neurons. We used cortical neurons differentiated from various iPSCs as a model based on our previous findings of transcriptional and synaptic dysregulation in these neurons in a *DISC1*-mutation dependent manner [33]. We also report the molecular and structural interactions between DISC1 and ATF4. Together, these results reveal a novel mechanism of action by DISC1–ATF4 in transcriptional regulation and provide insight into the pathogenesis of psychiatric disorders.

Materials and methods

Human iPS cell culture and cortical neural differentiation

Human iPSC lines (D2: a schizophrenia patient line with 4 base-pair deletion of *DISC1*; C3: a sibling control line from the same family as D2; D2R: an isogenic iPSC line, in which the *DISC1* mutation was corrected in the D2 iPSC line by genome editing in the previous study [33]; and D2-ATF4$^{+/-}$: ATF4 heterozygous deletion line from the D2 iPSC line, generated in the current study) were maintained in human iPSC media on MEF as previously described [33]. Cortical neuron differentiation from human iPSCs was adapted from our previously established protocol [33]. Briefly, iPSC colonies were detached from the feeder layer with 1 mg/ml collagenase and suspended in embryonic body (EB) medium, consisting of FGF-2-free iPSC medium supplemented with 2 µM Dorsomorphin and 2 µM A-83, in nontreated polystyrene plates for a week. On day 7, the floating EBs were attached onto matrigel-coated six-well plates in neural induction medium (NPC medium) containing 2 µM cyclopamine to form neural tube-like rosettes. On day 22, the rosettes were picked mechanically and transferred to low attachment plates (Corning) to form neurospheres in NPC medium. The neurospheres were then dissociated with Accutase and plated onto matrigel-coated plates/coverslips in neuronal culture medium, consisting of 1 µM cAMP, 200 ng/ml L-ascorbic acid, 10 ng/ml BDNF, and 10 ng/ml GDNF.

ATF4 heterozygous knockout in iPSCs with the CRISPR/Cas9 system

The guide RNA primers were designed as shown in Supplementary Table 1b and cloned into the cloning vector (Addgene, Plasmid #41824) with Gibson Assembly Cloning Kit (New England Biolabs, E5510S). For targeting, 2×10^6 D2-iPSCs were electroporated with pCas9_GFP (8 µg) (Addgene, Plasmid #44719) and gRNAs (6 µg/each) using a P3 Primary Cell 4D-Nucleofector X Kit (Lonza) and Nucleofector 4D Device (Lonza) following the manufacturer's instructions. GFP positive cells were harvested 2–3 days after nucleofection with FACS sorting, and replated sparsely into a six-well plate (300–500 cells/well) for clonal isolation. Single clones were manually selected for PCR using the screening primers (Supplementary Table 1b) and clonal expansion. Positive clones were further confirmed by DNA Sanger sequencing and western blot.

Lentiviral vector construction and transfection

Human ATF4 cDNA sequence was cloned into the lentiviral vector under the control of human Ubiquitin C promoter (cFUGW: Addgene, plasmid #14883) as previously described [34]. The sequence-verified plasmid was cotransfected with Δ8.9 and VSVG vectors into HEK293FT cells using Lipofectamine 2000 (Thermo Fisher Scientific). Media containing virus particles were harvested until 72 h after transfection, centrifuged at 500 *g* for 10 min to remove cell debris, filtered (0.45-μm pore size), and then ultracentrifuged at 112,000 *g* for 2 h. Pellets were resuspended in neuronal medium, aliquoted and stored at −80 °C. Three-week-old neurons derived from C3 and D2R iPSC lines were infected with viral supernatant and cultured for one more week for experiments.

Fractionation, protein extraction, and western blot analysis

To extract proteins from whole cells, human iPSCs were lysed in RIPA buffer (150 mM NaCl, 1% Triton X-100, 0.5% sodium deoxycholate, 0.1% SDS; 50 mM Tris, pH 8.0) containing Complete Protease Inhibitor Cocktail (Roche). Samples were placed on ice for 30 min and sonicated briefly. The insoluble fraction was removed by centrifugation at 15,000 rpm for 15 min at 4 °C. To purify nuclear soluble, chromatin-bound fractions from human iPSCs, the Subcellular Protein Fractionation Kit (Thermo Fisher Scientific) was used according to the manufacturers' instructions.

For western blotting, protein concentrations were determined using the Bradford assay (BioRad). Equal amounts of protein were separated by 10% SDS-PAGE, transferred to nitrocellulose membranes (BioRad), and subsequently incubated with primary (Supplementary Table 1a) and secondary antibodies and visualized with SuperSignal West Dura Chemiluminescent Substrate (Thermo Scientific). Quantification of band intensities was performed using ImageJ software.

RNA isolation, qPCR, and RNA-seq analysis

Total cellular RNA was isolated with mirVana kit (Invitrogen) according to manufacturer's instructions. For qPCR, a total of 1 μg RNA was used to synthesized cDNA with the SuperScript III First-Strand Synthesis System (Invitrogen), followed by qPCR analysis [33]. All gene-specific primers used for the current study are summarized in Supplementary Table 1b.

For RNA sequencing, libraries were generated from 1 μg of total RNA from three biological replicates of 4-week-old forebrain neurons using the NEBNext® Poly(A) mRNA Magnetic Isolation Module (NEB) following the manufacturer's protocol. An Agilent 2100 BioAnalyzer and DNA1000 kit (Agilent) were used to quantify amplified cDNA and to control for the quality of the libraries. A qPCR-based KAPA library quantification kit (KAPA Biosystems) was applied to accurately quantify library concentration. Illumina HiSeq2500 was used to perform 100-cycle SR sequencing. Preprocessing of RNA-seq reads was performed using the FASTX toolkit (http://hannonlab.cshl.edu/fastx_toolkit/). Briefly, adapters were clipped, poor quality reads were filtered out, and identical reads were collapsed. Preprocessed reads were then aligned to the human genome (build GRCh37/hg19) using Tophat2 with default settings [35]. Raw gene counts were obtained using htseq-count from the HTSeq library [36] and differential gene expression analysis was performed using the R statistical package DESeq2 [37], which uses linear modeling and variance reduction techniques for estimated coefficients to test individual null hypotheses of zero $\log_2$-fold changes between two conditions (ATF4 overexpression over wild type). For identifying differentially expressed genes, an FDR of 0.05 was used and a fold change threshold was set at log2 (fold change) > ±1 (Supplementary Table 2). Gene ontology (GO) analyses on biological processes were performed by the Database for Annotation, Visualization, and Integrated Discovery v6.8 [38]. KEGG pathway analyses were performed by the WEB-based Gene SeT Analysis Toolkit (WebGestalt) update 2017 [39]. Plots were generated using R version 3.4.3 with the ggplot2 package [40]. The plot size of individual circles is determined by the percentage of genes within each ontology/pathway group that is present in the query gene list, and the color is determined by the *P* value for gene enrichment for each ontology/pathway term.

ChIP-qPCR analysis

Two million neurons were collected and subjected to chromatin IP with antibodies to ATF4 (C-20, Santa Cruz), or normal Rabbit IgG (Cell Signaling) as a control following procedures as described [41]. Specific primers for gene promoter regions (Supplementary Table 1b) were used in qPCR to detect the enrichment of specific DNA sequences in the ATF4 bound chromatin fraction.

Immunocytochemistry

Cells were fixed with 4% paraformaldehyde (Sigma) for 15 min at room temperature, and then permeabilized and blocked with 0.25% Triton X-100 (Sigma) and 10% donkey serum in PBS for 20 min. Samples were incubated with primary antibodies (Supplementary Table 1a) at 4 °C overnight, followed by incubation with secondary

antibodies for 1 h at room temperature. Images were captured with identical settings for parallel cultures using Zeiss LSM 800 confocal microscope, or Zeiss Axiovert 200 M microscope, and analyzed with ImageJ (NIH). To calculate synaptic bouton density, total $SV2^+$ puncta in a given image were counted by ImageJ Analyze Particles, and the total dendritic length was measured by ImageJ plugin NeurphologyJ [42]. The synaptic density was determined by D (D = total $SV2^+$ puncta/total dendritic length).

MEA analysis

Twelve-well multielectrode array (MEA) plates (Axion Biosystems) were used and each well contained an 8×8 grid of 30 nm circular nanoporous platinum electrodes. Wells were coated with PDL and laminin and neurons were plated at a density of 500,000 neurons/well. MEA plates with neurons were cultured at 37 °C and 5% CO_2, and cells were fed every week by neuronal differentiation media (BrainPhys Neuronal Medium N2-A & SM1 kit (STEMCELL), 2 mM L-glutamine, B27, 1 µM cAMP, 200 ng/ml L-ascorbic acid, 10 ng/ml BDNF, and 10 ng/ml GDNF). Extracellular recordings of spontaneous action potentials were performed in culture medium at 37 °C using a Maestro MEA system and AxIS software (Axion Biosystems). Data were sampled at the rate of 12.5 kHz with a hardware frequency bandwidth of 200–5000 Hz. For spike detection, the threshold was set to six times the rolling standard deviation of the filtered field potential on each electrode. Five-minute recordings were used to calculate average spike rate and the number of active electrodes in each well. An active electrode was defined as spike rates ≥ 0.5/min.

Luciferase activity assay

SH-SY5Y cells were plated at a density of 2.5×10^5 cells per ml in 96-well plates 1 day before cotransfection with a plasmid expressing Renilla luciferase under the control of a human thymidine kinase 1 promoter (pRL-TK; Promega), and a plasmid expressing Firefly luciferase within the pGL4.20 backbone under the control of SYNPR or GRIN1 promoters at a ratio of 1:50. For assays comparing ATF4 target activation, cells were cotransfected with ATF4 vector within the pRK5 backbone at the indicated amount. Assays were conducted 2 days after transfection using the dual-luciferase reporter assay kit (Promega) according to the protocol.

Data collection and statistics

Results in Figs. 1e, f, 2b, e, Supplementary Figs. 1c, 2d, 4, and 5f were expressed as mean ± s.e.m. T-tests were performed, and the significance was indicated by asterisks in each plot. Kolmogorov–Smirnov test was performed in Fig. 2d. Chromatin immunoprecipitation sequencing (ChIP-seq) data in Supplementary Fig. 1b was collected from Gene Transcription Regulation Database v18.1 (http://gtrd.biouml.org). Enrichment analysis for the overlap between transcription factor binding genes and differentially expressed genes in D2 was performed by Fisher's exact test. The universe for the Fisher's exact test was defined as all genes with raw counts > 10 in at least one sample of the DISC1 dataset, and only transcription factor targets present in this universe (expressed in the DISC1 dataset) were considered for the analysis. DISC1 interactors and transcription factors in Supplementary Fig. 1a were collected from BioGRID 3.4 (https://thebiogrid.org/118061/summary/homo-sapiens/disc1.html) and TFCat (http://www.tfcat.ca/index.php). RNA sequencing data of D2 over C3 were collected from our previous study and analyzed as previously described [33].

Constructs and protein expression

The various coding sequence of DISC1 (NP_777279.2) and ATF4 (NP_033846.2) were PCR amplified and cloned into a modified pET32a vector. Recombinant proteins were expressed in BL21 (DE3) *Escherichia coli* cells. The N-terminal His_6-tagged proteins were purified using Ni^{2+}-nitrilotriacetic acid agarose column followed by size-exclusion chromatography (Superdex 200 column from GE Healthcare) in the final buffer of 50 mM Tris-HCl (pH 7.8), 100 mM NaCl, 1 mM DTT, and 1 mM EDTA. For NMR structure determination, ATF4 leucine zipper domain (residues 314–349; ATF4-LZ) was fused to the C-terminal end of DISC1-CC (coiled coil, residues 765–835) with a 26 amino acids linker (natural sequence GEASASYPTAGAQETEA from DISC1 836–852 plus thrombin cleavable linker LVPRGSGFG).

Isothermal titration calorimetry (ITC) assay

ITC measurements were carried out on a MicroCal VP-ITC calorimeter at 25 °C. Titration buffer contained 50 mM Tris-HCl (pH 7.8), 100 mM NaCl, 1 mM EDTA, and 1 mM DTT. For a typical experiment, each titration point was performed by injecting a 10 µl aliquot of a protein sample (at 200 µM) from a syringe into a protein sample in the cell (at 20 µM) at a time interval of 120 s to ensure that the titration peak returned to the baseline. The titration data were analyzed by Origin 7.0 and fitted by a one-site binding model.

Analytical gel filtration chromatography coupled with static light scattering

This analysis was performed on a fast protein liquid chromatography (FPLC) system coupled with a static light

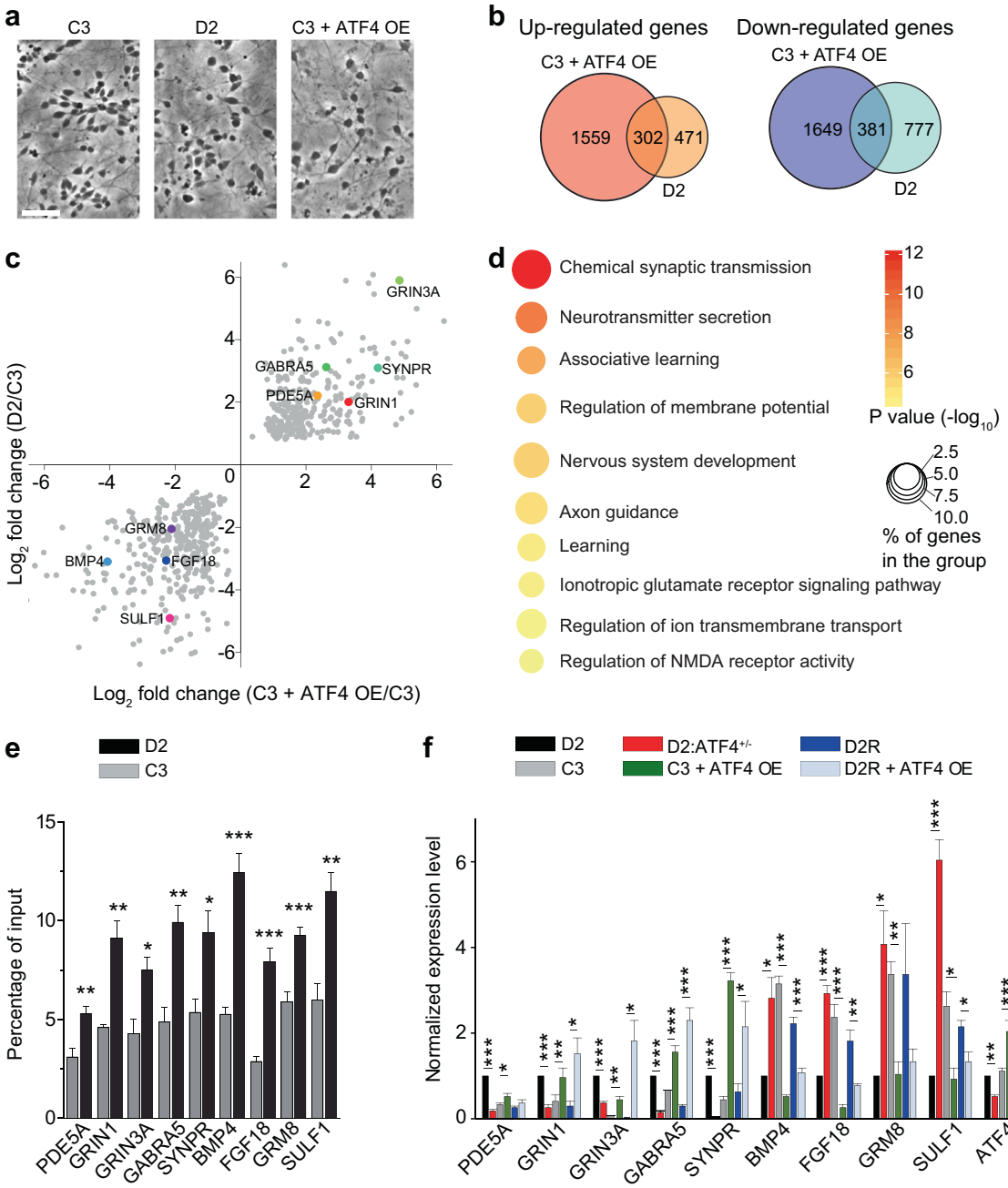

Fig. 1 ATF4 directly regulates the expression of a large set of dysregulated genes in *DISC1* mutant human neurons. **a** Sample images of neurons derived from different iPSC lines. Scale bar, 50 µm. **b** Venn diagrams showing significant overlap of dysregulated genes in control neurons with ATF4 overexpression (C3 + ATF4 OE) and in D2 cortical neurons. **c** Scatter plot of commonly dysregulated genes in C3 + ATF4 OE and D2 neurons. Highlighted in different colors are genes subjected to further validation and investigation. **d** GO analysis of 302 commonly upregulated genes in C3 + ATF4 OE and D2 neurons. Bubble plot showing enrichment for biological process terms related to synaptic function. Size and color of the bubble represent the proportion of commonly dysregulated genes enriched in each pathway (%) and the significance of enrichment, respectively. **e** ChIP-qPCR analysis of ATF4 binding at the promoter regions of indicated genes in C3 and D2 neurons, note the enhanced binding of ATF4 to these gene promoters in D2 neurons. Values represent mean ± s.e.m. ($n = 3$, $^{*}p < 0.05$, $^{**}p < 0.01$, $^{***}p < 0.001$, t-test). **f** Relative mRNA expression of commonly dysregulated genes in D2, C3, D2:ATF4$^{+/-}$, C3 + ATF4 OE, D2R, and D2R + ATF4 OE cortical neurons. Values represent mean ± s.e.m. ($n = 3$, $^{*}p < 0.05$, $^{**}p < 0.01$, $^{***}p < 0.001$, t-test)

scattering detector (miniDAWN; Wyatt) and a differential refractive index detector (Optilab; Wyatt). Protein samples (100 µl, concentration of 200 µM) were loaded to a Superose 12 10/300 GL column (GE Healthcare) preequilibrated with assay buffer containing 50 mM Tris-HCl (pH 7.8), 100 mM NaCl, 1 mM EDTA, and 1 mM DTT on an AKTA FPLC system (GE Healthcare). Data were analyzed with Astra 6 (Wyatt).

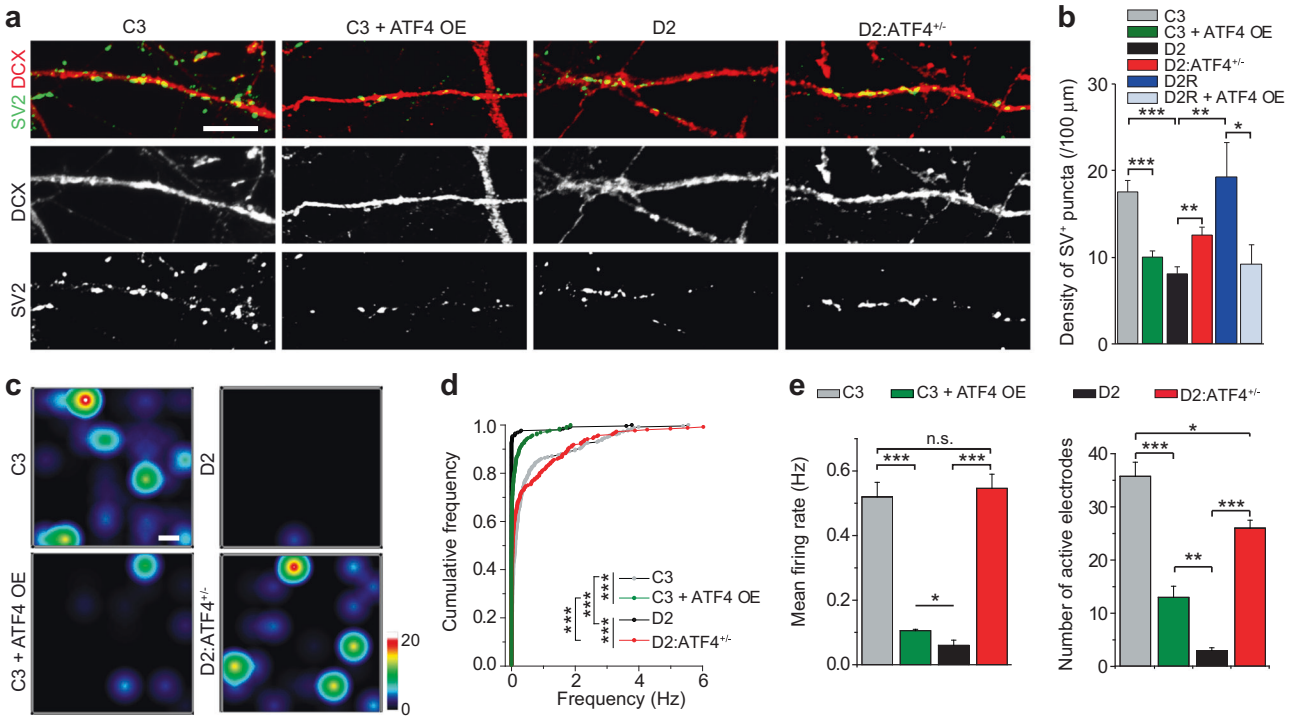

Fig. 2 ATF4 is essential for synaptic function in human neurons. **a** Sample confocal images of neuronal processes of 4-week-old neurons from different iPSC lines immunostained with SV2 (green) and DCX (red). Scale bar, 20 µm. **b** Quantification of densities of $SV2^+$ puncta. Values represent mean ± s.e.m. ($n = 3$, $^*p < 0.05$, $^{**}p < 0.01$, $^{***}p < 0.001$, *t*-test). **c** Heat map of MEA recordings visualized with Axion BioSystems Integrated Studio (AxIS). Active channels represented by color coded dots on the map. Scale bar: 200 µm. Also see Supplementary Movie 1. **d** Quantification of cumulative frequency. ($n = 3$; $^{***}p < 0.001$, Kolmogorov–Smirnov test). **e** Quantification of mean firing rate and number of active electrodes under different conditions. Values represent mean ± s.e.m. ($n = 3$, $^*p < 0.05$, $^{**}p < 0.01$, $^{***}p < 0.001$, *t*-test)

DNA binding assay

Complementary oligonucleotides were resuspended with an annealing buffer (10 mM Tris pH 7.8, 50 mM NaCl, and 1 mM EDTA) and adjusted to 100 µM. A pair of complementary oligonucleotides at an equal volume were mixed in an eppendorf tube. The mixture was boiled in a water bath for 5 mins and then cooled down to room temperature. The annealed double-strand DNA solution was subsequently exchanged into the binding buffer composed of 50 mM Tris-HCl (pH 7.8), 100 mM NaCl, 1 mM DTT, and 1 mM EDTA using a PD-10 desalting column (GE Healthcare). For the ITC binding assay, double-stranded DNA (GCAGATGACGTCATCTGC) at 65 µM was titrated into ATF4 278–349 alone or mixed with an equal molar amount of DISC1-CC or L822Q-DISC1-CC mutant at 13 µM in the binding buffer.

NMR spectroscopy

NMR samples contained 0.8 mM of the DISC1/ATF4 protein in 100 mM potassium phosphate (pH 6.5, with 1 mM DTT, 1 mM EDTA) in 90% H_2O/10% D_2O or 99.9 D_2O. NMR spectra were acquired at 30 °C on Varian Inova 750- and 800-MHz spectrometers each equipped with an actively z-gradient shielded triple resonance cryo-probe. Backbone and side-chain resonance assignment of DISC1/ATF4 was achieved by the standard heteronuclear correlation experiments.

For the ^{1}H NMR spectrum analysis of ATF4/DNA interaction, the sample contained 0.1 mM double-strand DNA (GCAGATGACGTCATCTGC) in 50 mM Tris-HCl (pH 7.8), 100 mM NaCl, 1 mM DTT, and 1 mM EDTA. ATF4, DISC1-CC, and L822Q-DISC1-CC mutant were titrated into the dsDNA step by step. NMR spectra were acquired at 10 °C on Varian Inova 800-MHz spectrometers each equipped with an actively z-gradient shielded triple resonance cryo-probe.

NMR structural calculation

Interproton distance restraints were obtained from a suite of three-dimensional, ^{13}C-and ^{15}N-separated NOESY experiments using a mixing time of 80 ms. Hydrogen bonding restraints were generated from the standard secondary structure of the protein based on the nuclear Overhauser enhancement (NOE) patterns (ϕ and ψ angles) derived from the chemical shift analysis program TALOS [43]. Structures

were calculated using the program CNS [44]. Figures were generated using PYMOL (http://pymol.sourceforge.nt/) and MOLMOL [45]. The program Procheck was used to assess the overall quality of the structures [46]. Ramachandran statistics for the final ensemble of structures for residues 776–801, 805–830 of DISC1 and residues 316–340 of ATF4 show that 98.6% of residues are in the most favored region, 1.3% of the residues are in the additionally allowed region, and 0.1% of the residues are in the generally allowed region. None of the structures exhibits distance violations >0.3 Å or dihedral angle violations >4° (Supplementary Table 3).

Results

ATF4 directly regulates the expression of a large set of dysregulated genes in *DISC1* mutant human cortical neurons

We have previously generated iPSC lines from a patient with schizophrenia and a *DISC1* 4 base-pair deletion mutation (D2 line) and from a healthy sibling without the *DISC1* mutation (C3 line) [47], and RNA-seq analysis identified a large set of dysregulated genes in cortical neurons differentiated from the D2 line (D2 neurons hereafter) compared with C3 neurons [33]. To understand how mutant DISC1 leads to dysregulated gene expression in human neurons, we first tried to identify potential transcription factors that bind to DISC1, as DISC1 lacks a DNA-binding domain. Eight transcription factors were identified as potential binding partners of DISC1 based on the DISC1 interactome [18] (Supplementary Fig. 1a). By comparing the available ChIP-seq datasets of ATF4, MYF6, MYT1L, NCOR1, and dysregulated genes in RNA-seq dataset from *DISC1* mutant neurons, we found that the most significant overlap was between ATF4 ChIP targets and dysregulated genes in D2 neurons ($p = 3.848e{-}07$; Supplementary Fig. 1b). Interestingly, a similar comparison between RNA-seq in D2 neurons and ChIP-seq targets of three C/EBP members, which share a high sequence identity with ATF family proteins, did not show any significant overlap. Together with previous findings that DISC1 regulates ATF4 transcriptional activity when exogenously expressed [31] and in mouse hippocampal neurons [30], these results raised the possibility that dysregulated ATF4 function may contribute to transcriptional changes in *DISC1* mutant neurons.

Since disease-relevant nonsynonymous *DISC1* variants were shown to affect ATF4 nuclear targeting when expressed in cell lines [32], we first asked the question whether the localization of ATF4 protein is affected by the *DISC1* mutation. While the total protein level of ATF4 in D2 iPSCs was comparable with that in control C3 iPSCs, ATF4 showed a significant increase in the nucleus fraction in D2 iPSCs, with a more pronounced presence in the chromatin bound form (Supplementary Fig. 1c). These results suggest that increased ATF4 in the nucleus may affect the expression of target genes. We tested this idea by overexpressing ATF4 in human cortical neurons differentiated from C3 iPSC line (Fig. 1a). We confirmed that our differentiation protocol [33] led to highly enriched glutamatergic cortical neurons from both C3 and D2 iPSC lines (Supplementary Fig. 2). RNA-seq analysis revealed that C3 iPSC-derived cortical neurons with ATF4 overexpression (C3 + ATF4 OE) showed large-scale gene expression changes compared with that of C3 neurons (Supplementary Table 2). Interestingly, a large set of genes are similarly dysregulated in C3 + ATF4 OE and D2 neurons, including 39% of upregulated genes and 33% of downregulated genes in D2 neurons (Fig. 1b), and the expression changes are highly correlated (Fig. 1c and Supplementary Fig. 3a, b). GO analysis of 302 commonly upregulated genes showed enrichment for synaptic transmission, neurotransmitter release, and nervous system development (Fig. 1d). GO analysis of 381 commonly downregulated genes shows enrichment for extracellular matrix organization and cell adhesion (Supplementary Fig. 3c). We also performed KEGG pathway analysis for differentially expressed genes. Eight out of the top ten pathways are shared for upregulated genes, including terms for "GABAergic synapse" and "glutamatergic synapse" (Supplementary Fig. 3d), while six out of the top ten pathways are shared for downregulated genes, including terms for "ECM-receptor interaction" and "focal adhesion" (Supplementary Fig. 3e). Taken together, these results suggest that elevated ATF4 levels in control human cortical neurons recapitulate the main features of transcriptomic dysregulation observed in *DISC1* mutant neurons.

To determine that gene expression is transcriptionally regulated by direct ATF4 binding in human cortical neurons, we first performed ChIP-PCR for a subset of nine genes in C3 and D2 neurons (five common upregulated synaptic genes and four common downregulated neurodevelopmental genes in D2 and C3 + ATF4 OE; Fig. 1c). We detected enriched ATF4 binding in promoter regions of these genes in both C3 and D2 neurons, but with significantly higher levels in D2 neurons (Fig. 1e). The gene expression changes of these nine genes were also validated using qPCR from independent samples (Fig. 1f). We further confirmed our finding using cortical neurons derived from the isogenic D2R iPSC line, in which the *DISC1* mutation was corrected via genome editing [33] and D2R neurons with ATF4 overexpression (Fig. 1f). Furthermore, we used a luciferase reporter assay to validate that increased ATF4 levels at promoter regions of *SYNPR* and *GRIN1* led to

increased reporter expression (Supplementary Fig. 4). These results suggest that the increased presence of ATF4 in the nucleus and binding at promoter regions mediates transcriptional dysregulation in *DISC1* mutant neurons.

We next determined whether decreasing ATF4 levels could rescue dysregulated gene expression in D2 neurons. We used CRISPR/Cas9 to generate an isogenic iPSC line with *ATF4* heterozygous knockout. Two independent gRNAs spaced out by 472 base pairs, with one targeted at the end of Exon 1 and the other one in the middle of Exon 2, were designed for *ATF4* gene targeting (Supplementary Fig. 5a). Deletion accuracy was confirmed by genomic DNA Sanger sequencing (Supplementary Fig. 5b). Basic characterization did not show any differences in pluripotency gene expression or neuronal differentiation of the D2:ATF4$^{+/-}$ line (Supplementary Fig. 5c, d). In the isogenic D2:ATF4$^{+/-}$ line, the total ATF4 protein level was reduced to about half of that in D2 line (Supplementary Fig. 5e). Furthermore, the chromatin-bound ATF4 level in D2:ATF4$^{+/-}$ cells was decreased to a level similar to that in C3 cells (Supplementary Fig. 5f). Importantly, decreasing ATF4 levels partially normalized dysregulated gene expression in D2 neurons, including both upregulated and downregulated genes (Fig. 1f). Collectively, these results identify ATF4 as a key mediator for DISC1-dependent gene regulation in human cortical neurons.

ATF4 regulates synaptic function in human neurons

As the top ten GO terms for upregulated genes identified in D2 and C3 + ATF4 OE are almost all related to synaptic function (Fig. 1d), we next investigated whether ATF4-dependent gene regulation is functionally involved in synaptic development. We confirmed previous findings that D2 neurons exhibit a decreased density of SV2^{+} synaptic puncta compared with C3 and D2R neurons [33] (Fig. 2a, b). Importantly, ATF4 OE in C3 or D2R neurons phenocopied the synaptic deficits in D2 neurons, while ATF4$^{+/-}$ in D2 neurons largely rescued the phenotype (Fig. 2a, b).

We further examined the synaptic network properties using MEA recordings. Spontaneous neuronal firing became evident in neurons cultured for 4 weeks (Fig. 2c). Consistent with results from the morphological analyses of synapses, the network activity was significantly lower in D2 neurons compared with C3 neurons, with reduced mean firing frequency, as well as lower numbers of active electrodes (Fig. 2c–e and Supplementary Movie 1). Moreover, the network activity in C3 + ATF4 OE neurons resembled that of D2 neurons, whereas D2:ATF4$^{+/-}$ neurons were more similar to C3 neurons (Fig. 2c–e). Thus, ATF4 is also a key mediator for DISC1-dependent regulation of synaptic functions in human neurons.

High-resolution structure of the DISC1/ATF4 complex

It has been suggested that DISC1 and ATF4 form a transcriptional repression complex and suppress gene expression in a DISC1-dependent manner [30]. We previously showed that in D2 neurons, the DISC1 protein level is largely depleted [33]. However, the detailed mechanisms of how *DISC1* mutation and protein depletion can lead to elevated levels of ATF4 protein in the nucleus and at the chromatin-bound state is largely unknown. To address this question, we first characterized the interaction between DISC1 and ATF4. We obtained highly homogeneous DISC1 protein only missing the N-terminal 321 residues, which is predicted to be unstructured and not required for ATF4 binding (Fig. 3a) [29]. The predicted helical region of DISC1 (residues 322–852) [19, 21] was found to bind to the ATF4 leucine zipper domain (residues 314–349; ATF4-LZ) with a Kd of ~14 nM and a stoichiometry of 1:1 (Fig. 3b), indicating that ATF4 is a highly specific DISC1 interactor. Detailed truncation mapping coupled with isothermal titration calorimetry (ITC)-based quantitative binding experiments allowed us to map a C-terminal fragment (residues 765–835) (DISC1-CC; Fig. 3a), a predicted coiled coil domain, as the minimal and complete ATF4-LZ binding domain (Fig. 3b). A gel-filtration coupled with static light scattering analysis revealed that both DISC1-CC and ATF4-LZ in their isolated states formed dimers in solution and the DISC1-CC/ATF4-LZ adopted a stable heterodimer (Fig. 3c and Supplementary Fig. 6a).

To elucidate the molecular mechanism governing the specific DISC1/ATF4 interaction, we determined the high-resolution solution structure of the DISC1-CC/ATF4-LZ complex by NMR spectroscopy (Fig. 3d, e and Supplementary Table 3). Determination of the structure of the DISC1-CC/ATF4-LZ complex was aided by connecting ATF4-LZ to the C-terminal end of DISC-CC with a nine amino acids (LVPRGSGFG) flexible linker, as this has greatly simplified the assignment of the intermolecular NOE signals. The covalent fusion of DISC-CC with ATF4-LZ did not have an obvious conformational impact on the complex structure, as the NMR spectra of DISC1-CC in the fusion protein and in the mixture with ATF4-LZ were essentially identical (Supplementary Fig. 6b, c). The DISC1-CC/ATF4-LZ complex formed a three-helix bundled coiled-coil structure, in which DISC1-CC formed an antiparallel helix-turn-helix structure with a 4-residue linker and ATF4-LZ adopted a single α-helix and extensively interacted with the two DISC1 helices (Fig. 3e and Supplementary Fig. 7e). The ATF4 binding surface of DISC1-CC is extremely conserved (Supplementary Fig. 7a, c) and largely hydrophobic (Supplementary Fig. 7d). Correspondingly, the residues of ATF4-LZ that are involved in

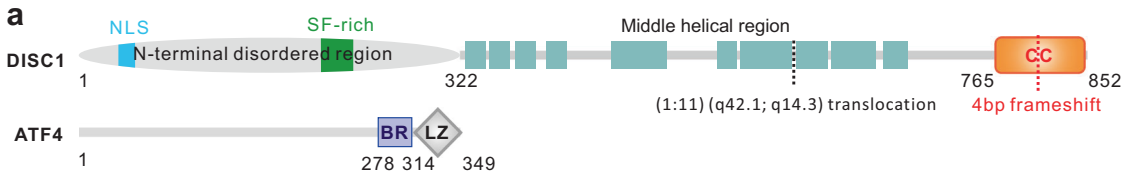

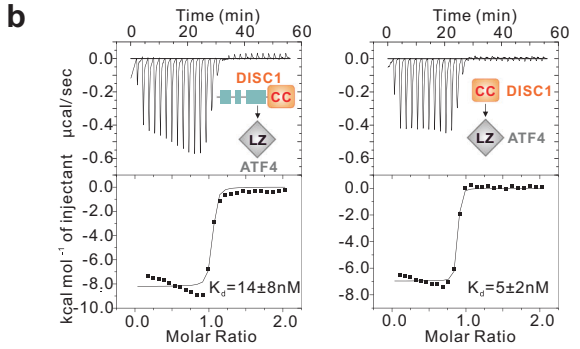

c

	Theoretical MW (kD)	Measured MW (kD)	Binding Mode
ATF4	18.6	35.5 ± 0.1	LZ LZ
DISC1	10.0	19.0 ± 0.2	CC CC
ATF4+ DISC1	28.6	28.2 ± 0.1	LZ CC

f

DISC1 CC	ATF4 LZ	Kd (μM)
WT	WT	0.005 ± 0.002
L822Q	WT	not detectable
L789Q	WT	not detectable
WT	L332Q	5.6±0.3

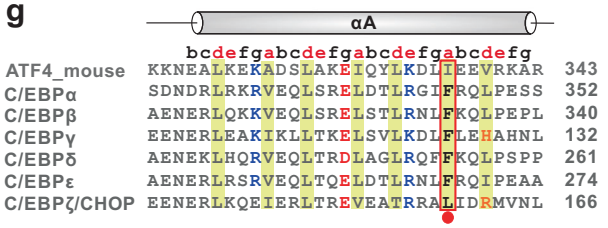

h

DISC1	TFs	K_d (μM)
WT	ATF4	0.005 ± 0.002
WT	C/EBPα	11 ± 1
WT	C/EBPζ	10 ± 5

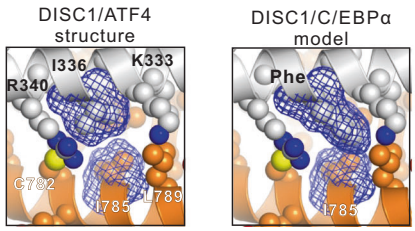

binding to DISC1-CC are also extremely conserved (Supplementary Fig. 7b).

All three helices in the DISC1-CC/ATF4-LZ complex adopt a canonical heptad repeat structure. The residues at the "a" and "d" positions of all heptad repeats are composed of hydrophobic residues (Supplementary Fig. 7f), and these residues are chiefly responsible for forming the hydrophobic core of the coiled-coil helix bundle in an interaction mode known as "knobs into holes" (Supplementary Fig. 7d). Single amino acid substitutions of several of these hydrophobic residues either in DISC1 or in ATF4 can significantly weaken or even disrupt the DISC1/ATF4 interaction (Fig. 3f and Supplementary Fig. 8a–c). In addition to the hydrophobic interactions, several pairs of charge–charge interactions mediated by residues at the "e" and "g" positions of the heptad repeats also play important roles for the DISC1/ATF4 complex formation, presumably by enhancing the specificity of the interaction (Supplementary Fig. 7f). The residues forming these specific charge–charge interactions are also highly conserved during the evolution for both proteins (Supplementary Fig. 7a–c).

The frameshift mutation (4-basepair deletion in the exon 12) of *DISC1* in the psychiatric disorder patients encodes a truncated DISC1 protein with the entire α2 helix removed

◀ **Fig. 3** DISC1 specifically interacts with ATF4. **a** Schematic diagram and amino acid sequence features of DISC1 and ATF4. DISC1 contains an N-terminal disordered region, a middle helical region, and a C-terminal predicted coiled-coil (CC) region. The position of a translocation break point t(1;11) at amino acid position 597 is highlighted with a dashed line in black, and the frameshift mutation in the CC region (D2) is indicated with a dashed line in red. ATF4 contains a basic DNA binding region (BR) and a leucine zipper (LZ) dimerization domain in its C-terminal end. **b** ITC-based measurements quantifying the binding affinities between DISC1 322–852 and ATF4-LZ and between DISC1 765–835 (DISC1-CC) and ATF4-LZ. Note that DISC1-CC is sufficient to interact with ATF4-LZ. **c** Analytical gel filtration chromatography analysis coupled with static light scattering based analysis of DISC1-CC, trx tagged-ATF4-LZ, and the DISC1-CC/trx tagged-ATF4-LZ complex. The theoretical and measured molecular weights and binding modes are listed. The results indicate that DISC1-CC can disrupt ATF4 homodimer and form a stable 1:1 complex with ATF4-LZ. **d** Stereo-view showing the backbones of 20 superimposed NMR structures of the DISC1-CC/ATF4-LZ complex. **e** Ribbon diagram of a representative NMR structure of the DISC1-CC/ATF4-LZ complex. **f** ITC-based measurements comparing the binding affinities between DISC1 (WT or mutant) and ATF4 (WT or mutant). Note that mutations in either DISC1-CC or ATF4-LZ disrupt the binding. **g** Sequence alignment of the C/EBP family transcription factors and ATF4, showing very high sequence identity (amino acids involved in hydrophobic interactions are highlighted in yellow, charged residues involved in positively charged interaction are colored in blue, and negatively charged colored in red). Ile336, which is critical for the highly specific ATF4/DISC1 interaction, and the corresponding residues in other family members are outlined with a box. **h** Summary of ITC-derived dissociation constants of the binding between DISC1 and some members of the C/EBP family transcriptional factors. **i** Combined ribbon and sphere representation showing the detailed interaction interface between Ile336 on ATF4-LZ with DISC1-CC. Left: Ile336 interacts with I785 and L789 from DISC1 through insertion of its sidechain into the hydrophobic core of DISC1-CC. Right: combined sphere and mesh model showing that substitution of Ile336 with Phe residue leads to the sidechain crash with I785 from DISC1

and with nine nonnative amino acids at the very end of the C terminal [48] (Fig. 3a and Supplementary Fig. 7a). Based on the structure of the DISC1/ATF4 complex determined here, the truncation of the α2 helix of DISC1 would certainly disrupt its binding to ATF4 as the single point substitution of Leu822 in this helix with Gln completely eliminated DISC1 binding to ATF4 (Fig. 3f and Supplementary Fig. 8a).

DISC1 specifically disrupts ATF4 dimer formation and DNA binding

The amino acid sequences of the leucine zipper domain of the basic leucine zip (b-ZIP) family transcriptional factors are highly homologous (Fig. 3g) and thus the members are known to be capable of forming both homo- and heterodimers. Available ChIP-Seq data showed that only ATF4, but not other three C/EBP members, showed a significant overlap in dysregulated gene expression with D2 neurons (Supplementary Fig. 1b). In order to understand why this DISC1 variant specifically affected ATF4-dependent gene regulation, it is necessary to answer one critical question: whether DISC1 specifically binds to ATF4 only or promiscuously binds to other members of the b-ZIP family as well? The C/EBP family of transcription factors shares very high sequence identities with ATF4 (Fig. 3g). Structure-based sequence analysis of the C/EBP family members reveals that, among the residues that form critical interactions with DISC1-CC, only one residue is unique to ATF4 (Ile336 in ATF4 vs. a more bulky Phe in the majority of the others). Surprisingly, the binding affinity between DISC1 and C/EBPα is ~2000-fold weaker than the DISC1/ATF4 interaction (Kd values of ~11 μM vs. 5 nM; Fig. 3h and Supplementary Fig. 8d), presumably due to the steric hindrance caused by the bulky Phe of C/EBPs (Fig. 3i). In addition, C/EBPζ (CHOP) has a favorable Leu in the position corresponding to Ile336 of ATF4, but with a charged Arg in the following d position instead of a hydrophobic Val (Fig. 3g). The binding affinity between ATF4 and C/EBPζ is also ~2000-fold weaker than the DISC1/ATF4 interaction (Fig. 3h and Supplementary Fig. 8d). Together, the above biochemical and structural analysis revealed that DISC1 is a very specific ATF4 binder and the binding specificity is encoded in its DISC1 binding leucine zipper sequence, which is subtly different from those of other C/EBP transcription factors.

ATF4 is a member of the CREB transcription factor family that is known to form dimers via its C-terminal LZ domain, and the LZ-mediated dimerization is essential for ATF4 to interact with palindromic dsDNA sequences with a very high affinity (Fig. 4a). As the DISC1 binding sequences of ATF4-LZ largely overlap with its dimerization region, and binding of DISC1 disrupts the ATF4 dimer formation (Fig. 3c and Supplementary Fig. 6a), it is envisioned that DISC1 can regulate ATF4's binding to its cognate dsDNA sequences. We tested this prediction using ITC-based quantitative binding assays. In the absence of DISC1, ATF4 binds to a canonical CRE promoter double strand DNA (GCAGATGACGTCATCTGC) with a Kd of ~12 nM (Fig. 4a). The addition of a stoichiometric amount of DISC1-CC led to ~500-fold reduction of ATF4's DNA binding affinity (Kd ~5 μM; Fig. 4b). As a control, the L822Q-DISC1-CC mutant, which is defective in binding to ATF4, had very little impact on the DNA binding of ATF4 (Fig. 4c). We further demonstrated by NMR spectroscopy that DISC1-CC, but not the L822Q-DISC1-CC mutant, can effectively release DNA from the ATF4/DNA complex by forming a DISC1-CC/ATF4 complex (Fig. 4d). In summary, our structure and biochemical studies reveal that wild-type DISC1, but not mutant DISC1, can effectively disrupt ATF4 homodimer formation, thereby significantly weakening ATF4's DNA binding affinity and specifically impacting ATF4-mediated transcriptions in a DISC1 dosage-dependent manner.

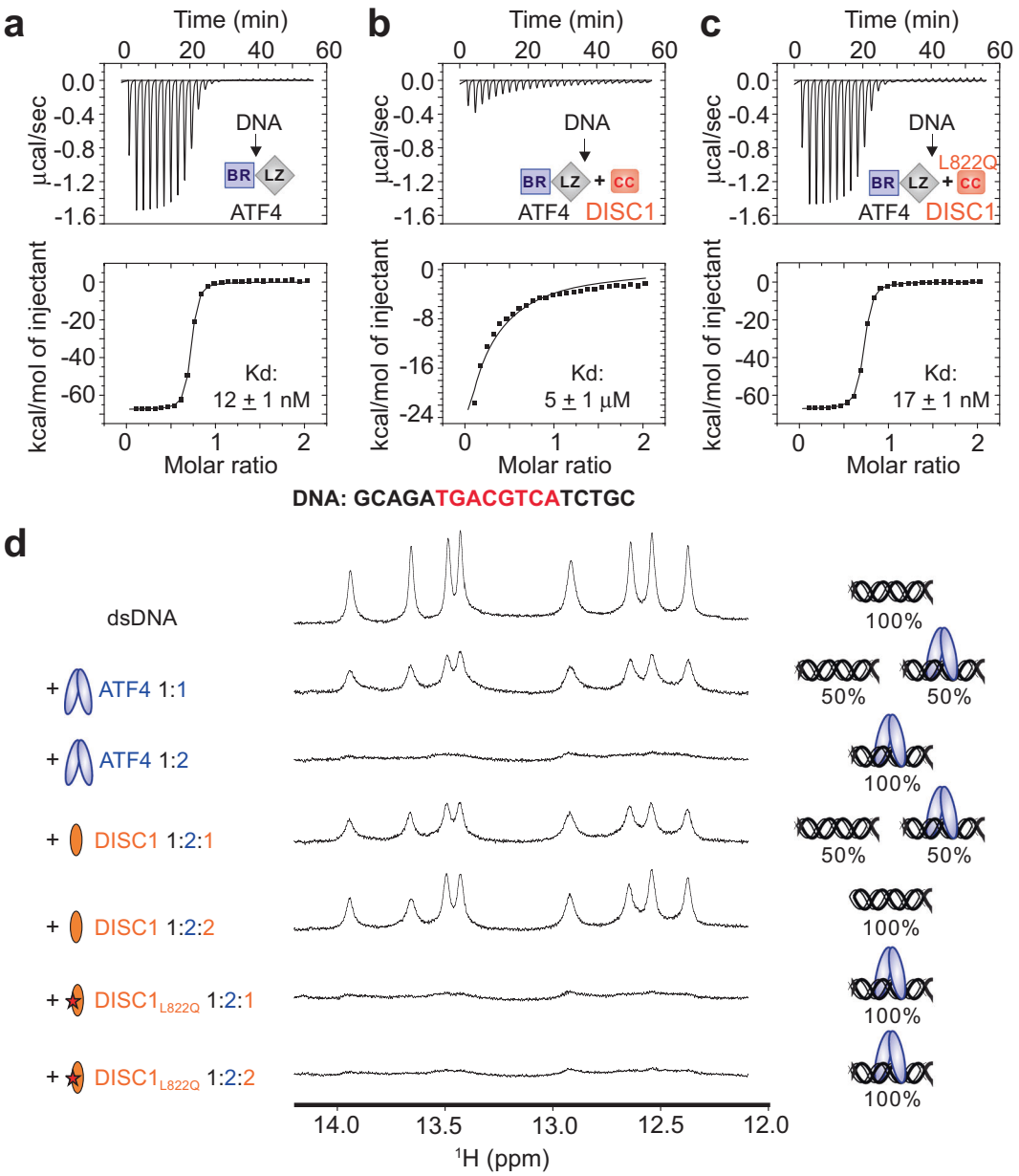

Together, these data lead us to propose a model in which wild-type DISC1 protein specifically binds to ATF4 protein with high affinity and releases ATF4 from chromatin DNA binding in control neurons; while in patient neurons, mutant DISC1 protein, with its binding domain disrupted, fails to interact with ATF4, and thus leads to excessive ATF4

◀ **Fig. 4** DISC1 prevents ATF4 from binding to DNA. **a**–**c** ITC-based measurements showing an ATF4 homodimer bound to double strand DNA (dsDNA: GCAGA**TGACGTCA**TCTGC) with a very strong affinity (**a**). Addition of equal molar amount of DISC1-CC (i.e. DISC1:ATF4 = 1:1) led to a ~500-fold reduction of the binding affinity between ATF4 and dsDNA (**b**), and the L822Q-DISC1-CC mutant did not affect the DNA binding ability of ATF4 (**c**). **d** 1D 1 H NMR spectra showing the imino proton resonances from the ATF4 binding dsDNA. Annealed double stranded DNA (**a**) was titrated with 1:1 and 1:2 molar ratios of ATF4, showing that the imino proton peaks of DNA are selectively broadened upon ATF binding. When DISC1-CC was added into the DNA/ATF4 complex from 1:1:2 ($DISC1_{WT}$: DNA: ATF4) to 2:1:2 molar ratio, the DNA was released from ATF4 as indicated by the recovery of its imino peaks. In contrast, addition of the L822Q-DISC1-CC mutant to the DNA/ATF4 complex from 1:1:2 ($DISC1_{L822Q}$: DNA: ATF4) to 2:1:2 molar ratio did not release DNA from ATF4. We did not calibrate the peak intensities of the NMR signals during the titrations, so that the signals representing the DISC1/ATF4 binding-induced DNA release appeared weaker due to the sample dilution upon adding DISC1. **e** A mechanistic model depicting DISC1 binding-induced inhibition of the ATF4/DNA interaction and ATF4-mediated transcriptional regulation

binding in chromatin DNA and global transcriptional dysregulation, which in turn causes neuronal synaptic defects (Fig. 4e).

Discussion

Although the interaction between DISC1 and ATF4, and its effect on the expression of selected genes has been reported in heterologous expression systems and in various animal models [28–31], whether such mechanisms are conserved in human neurons and contribute to disease relevant phenotypes are not known. In this study, we have biochemically characterized the functional and structural interaction properties between DISC1 and ATF4. The minimal domain required for the binding involves the coil-coil domain at the C-terminus of DISC1 (DISC1-CC; aa 765–852) and the leucine zipper domain of ATF4 (ATF4-LZ; aa 314–349). Moreover, we identified a novel mechanism for DISC1-dependent regulation of gene expression, in which high affinity and specific binding between wild-type DISC1 and ATF4 sequesters ATF4 from binding to DNA (Fig. 4e). A previous study used coimmunoprecipitation to show that the Exon 9-truncated DISC1 (deletion of aa 607–628) is deficient in its interaction with ATF4, indicating DISC1 Exon 9 is necessary for ATF4 binding [31]. Based on our previous study, this abrogated interaction by the deletion of Exon 9 is likely due to the deletion-induced DISC1 misfolding [23].

Proper subcellular localization and integration into functional molecular complexes is essential for protein function. DISC1, as a scaffold protein, has been shown to efficiently anchor proteins, like PDE4, Dynein, Kal-7, to precise subcellular locations [8]. On the other hand, aberrantly localized transcription factors, such as NF-kB, ATF2, and CREB, have been suggested to contribute to neurodegenerative diseases [49]. Early studies suggest that DISC1 regulates gene transcription through its direct presence in the nucleus, for instance, by colocalizing with promyelocytic leukemia bodies [31] or by forming a DISC1/ATF4 transcriptional repression complex [30]. In our patient-specific iPSC model with the *DISC1* 4 base-pair deletion at the C terminus, wild-type DISC1 protein is known to be largely depleted by mutant DISC1 protein [33]. Instead, we observed a significantly higher ATF4 distribution in the nucleus, especially in the chromatin bound fraction in *DISC1* mutant neurons. Together with our structural studies showing that DISC1 potently binds to ATF4 and thus sequesters ATF4 from binding to DNA, our results suggest that DISC1 serves as an important regulator controlling ATF4's availability in DNA binding in the nucleus, rather than its direct presence in the nucleus. This notion is further supported by a previous study showing that overexpressing wild-type DISC1 results in a reduced level of ATF5, a close homologue of ATF4, in the nucleus and redistribution in the cytoplasm [29].

Through manipulating ATF4 levels in wild type and *DISC1* mutant neurons, we demonstrated that ATF4 is a key mediator responsible for DISC1-dependent regulation at both transcriptional and synaptic functional levels (Figs. 1 and 2). Previous studies, such as those manipulating eIF2α phosphorylation to increase ATF4 protein [50, 51] or using a broad dominant-negative inhibitor of C/EBP family proteins including ATF4 [24], suggest that ATF4 negatively regulates synaptic plasticity. Our functional studies of human cortical neurons under different conditions confirmed an important role of ATF4 in synaptic function and further suggested that the level of ATF4 is fine-tuned for regulating synaptic function in neurons (Fig. 2). Moreover, our RNA-seq analyses in D2 neurons and C3 ATF4 OE neurons provide a direct mechanistic link between ATF4 target genes and synaptic function, as the top GO terms of dysregulated genes in both types of neurons are almost all linked to synaptic development and synaptic functions (Fig. 1d).

By solving the atomic structure of the complex formed between DISC1-CC and ATF4-LZ (Figs. 3 and 4), molecular insights can be gained on how deleterious variants damaging the integrity of DISC1-CC domain result in aberrant gene expression and deficits in cellular function. It is possible that mutant DISC1-mediated depletion of wild-type DISC1 can further promote the damaging effect [33]. The mutant DISC1-mediated wild-type DISC1 protein depletion would further increase the total amount of ATF4 dimer, and thus promote ATF4-mediated transcription (Fig. 4e). In addition, the depletion of wild-type DISC1 by the mutant copy may also alter the function of DISC1 binding proteins that interact with regions of DISC1 other than its C-terminal CC domain. DISC1-CC domain damage is commonly shared in disease-associated *DISC1* mutations, represented by the *DISC1* 4

base-pair deletion mutation in the American Pedigree H studied here, and chromosome (1:11) (q42.1; q14.3) translocation in the large Scottish family [52], and the recently found frameshift mutation from Ala595 in an ultra-rare variants study [53]. Thus, our study may provide a potential convergent mechanism underlying the *DISC1* mutation-related psychiatric disorders.

Eight transcription factors were identified as potential binding partners of DISC1 in the BioGRID3.4 database [18]. By comparing the available ChIP-seq datasets of four out of eight transcription factors (ATF4, MYF6, MYT1L, and NCOR1) and dysregulated genes in RNA-seq dataset from D2 neurons, the most significant overlap was found to be between ATF4 ChIP targets and dysregulated genes in D2 neurons. Interestingly, a similar comparison between RNA-seq in D2 neurons and ChIP-seq targets of three C/EBP members, which share a high sequence identity with ATF family proteins, did not show any significant overlap. This is consistent with our binding and structural analysis showing that DISC1/ATF4 binding is highly specific (Fig. 3g–i). Moreover, ATF4 appears to bidirectionally regulate gene expression, suggesting that ATF4 may be part of both activation and repression complexes. While some of the gene expression changes seen in D2 neurons may be secondary, our ChIP-PCR results validated direct binding of ATF4 to at least a subset of genes that are either upregulated or downregulated. Future studies are needed to identify the ATF4 binding partners that are involved in different complexes for gene expression regulation.

Recently, studies revealed a broader involvement of DISC1 dysregulation in pathological conditions outside psychiatric illnesses. Two studies indicated that disturbance of intrinsic soluble DISC1 protein participates in neurological diseases, partially through reducing synaptic protein expression [9, 10]. Another study implicated DISC1–ATF4 interactions in host immune responses against parasites in psychiatric patients [54]. Given that both DISC1 and ATF4 are critical functional proteins in multiple cell processes, our model could be a potential mechanism that broadly contributes to multiple disorders, particularly those involving psychiatric manifestations.

Acknowledgements We thank members of Ming and Song laboratories for discussion, D. Johnson and B. Temsamrit for technical support, J. Schnoll for lab coordination. This work was a component of the National Cooperative Reprogrammed Cell Research Groups (NCRCRG) to Study Mental Illness and was supported by the National Institutes of Health (NIH) grant to G-lM and HS (U19MH106434). Additional supports were by grants from RGC of Hong Kong (664113, AoE-M09-12, C6004-17G, T13-607/12 R, and T13-605/18 W to MZ; 16104518 to FY) and National Key R&D Program of China (2016YFA0501903 to MZ), and grants from NIH (P01NS097206 and R37NS047344 to HS, R35NS097370 and R01MH105128 to G-lM). MZ is a Kerry Holdings Professor in Science and a Senior Fellow of IAS at HKUST.

Author contributions XW and FY co-led the project and contributed equally to this work. ZW, ZG, CY, W-KH, FRR, YS, GZ, and KMC contributed to additional data collection and analyses, WZ contributed reagents, XW, FY, HS, MZ, and GM wrote the paper.

Compliance with ethical standards

Conflict of interest The authors declare that they have no conflict of interest.

Publisher's note: Springer Nature remains neutral with regard to jurisdictional claims in published maps and institutional affiliations.

References

1. Weinberger DR. Implications of normal brain development for the pathogenesis of schizophrenia. Arch Gen Psychiatry. 1987;44:660–9.
2. Mirnics K, Middleton FA, Lewis DA, Levitt P. Analysis of complex brain disorders with gene expression microarrays: schizophrenia as a disease of the synapse. Trends Neurosci. 2001;24:479–86.
3. Birnbaum R, Weinberger DR. Genetic insights into the neurodevelopmental origins of schizophrenia. Nat Rev Neurosci. 2017;18:727–40. https://doi.org/10.1038/nrn.2017.125
4. Sullivan PF, Daly MJ, O'Donovan M. Genetic architectures of psychiatric disorders: the emerging picture and its implications. Nat Rev Genet. 2012;13:537–51. https://doi.org/10.1038/nrg3240
5. Wen Z, Christian KM, Song H, Ming GL. Modeling psychiatric disorders with patient-derived iPSCs. Curr Opin Neurobiol. 2016;36:118–27. https://doi.org/10.1016/j.conb.2015.11.003
6. Soliman MA, Aboharb F, Zeltner N, Studer L. Pluripotent stem cells in neuropsychiatric disorders. Mol Psychiatry. 2017;22:1241–9. https://doi.org/10.1038/mp.2017.40
7. Chubb JE, Bradshaw NJ, Soares DC, Porteous DJ, Millar JK. The DISC locus in psychiatric illness. Mol Psychiatry. 2008;13:36–64.
8. Brandon NJ, Sawa A. Linking neurodevelopmental and synaptic theories of mental illness through DISC1. Nat Rev Neurosci. 2011;12:707–22.
9. Tanaka M, et al. Aggregation of scaffolding protein DISC1 dysregulates phosphodiesterase 4 in Huntington's disease. J Clin Investig. 2017;127:1438–50. https://doi.org/10.1172/JCI85594
10. Endo R, et al. TAR DNA-binding protein 43 and disrupted in schizophrenia 1 coaggregation disrupts dendritic local translation and mental function in frontotemporal lobar degeneration. Biol Psychiatry. 2018;84:509–21. https://doi.org/10.1016/j.biopsych.2018.03.008
11. Mao Y, et al. Disrupted in schizophrenia 1 regulates neuronal progenitor proliferation via modulation of GSK3beta/beta-catenin signaling. Cell. 2009;136:1017–31.
12. Duan X, et al. Disrupted-in-schizophrenia 1 regulates integration of newly generated neurons in the adult brain. Cell. 2007;130:1146–58. https://doi.org/10.1016/j.cell.2007.07.010
13. Faulkner RL, et al. Development of hippocampal mossy fiber synaptic outputs by new neurons in the adult brain. Proc Natl Acad Sci USA. 2008;105:14157–62. https://doi.org/10.1073/pnas.0806658105
14. Hayashi-Takagi A, et al. Disrupted-in-schizophrenia 1 (DISC1) regulates spines of the glutamate synapse via Rac1. Nat Neurosci. 2010;13:327–32.
15. Wang Q, et al. The psychiatric disease risk factors DISC1 and TNIK interact to regulate synapse composition and function. Mol Psychiatry. 2011;16:1006–23. https://doi.org/10.1038/mp.2010.87
16. Kim JY, et al. Interplay between DISC1 and GABA signaling regulates neurogenesis in mice and risk for

schizophrenia. Cell. 2012;148:1051–64. https://doi.org/10.1016/j.cell.2011.12.037
17. Seshadri S, et al. Interneuronal DISC1 regulates NRG1-ErbB4 signalling and excitatory-inhibitory synapse formation in the mature cortex. Nat Commun. 2015;6:10118. https://doi.org/10.1038/ncomms10118
18. Camargo LM, et al. Disrupted in schizophrenia 1 interactome: evidence for the close connectivity of risk genes and a potential synaptic basis for schizophrenia. Mol Psychiatry. 2007;12:74–86.
19. Soares DC, Carlyle BC, Bradshaw NJ, Porteous DJ. DISC1: structure, function, and therapeutic potential for major mental illness. ACS Chem Neurosci. 2011;2:609–32. https://doi.org/10.1021/cn200062k
20. Wilkinson B, et al. Endogenous cell type-specific disrupted in schizophrenia 1 interactomes reveal protein networks associated with neurodevelopmental disorders. Biol Psychiatry. 2018. https://doi.org/10.1016/j.biopsych.2018.05.009
21. Shao L, et al. Disrupted-in-schizophrenia-1 (DISC1) protein disturbs neural function in multiple disease-risk pathways. Hum Mol Genet. 2017;26:2634–48. https://doi.org/10.1093/hmg/ddx147
22. Thomson PA, et al. DISC1 genetics, biology and psychiatric illness. Front Biol. 2013;8:1–31.
23. Ye F, et al. DISC1 regulates neurogenesis via modulating kinetochore attachment of Ndel1/Nde1 during mitosis. Neuron. 2017;96:1041–1054 e1045. https://doi.org/10.1016/j.neuron.2017.10.010
24. Chen A, et al. Inducible enhancement of memory storage and synaptic plasticity in transgenic mice expressing an inhibitor of ATF4 (CREB-2) and C/EBP proteins. Neuron. 2003;39:655–69.
25. Ma T, et al. Suppression of eIF2alpha kinases alleviates Alzheimer's disease-related plasticity and memory deficits. Nat Neurosci. 2013;16:1299–305. https://doi.org/10.1038/nn.3486
26. Pasini S, Corona C, Liu J, Greene LA, Shelanski ML. Specific downregulation of hippocampal ATF4 reveals a necessary role in synaptic plasticity and memory. Cell Rep. 2015;11:183–91. https://doi.org/10.1016/j.celrep.2015.03.025
27. Davies G, et al. Study of 300,486 individuals identifies 148 independent genetic loci influencing general cognitive function. Nat Commun. 2018;9:2098. https://doi.org/10.1038/s41467-018-04362-x
28. Millar JK, Christie S, Porteous DJ. Yeast two-hybrid screens implicate DISC1 in brain development and function. Biochem Biophys Res Commun. 2003;311:1019–25.
29. Morris JA, Kandpal G, Ma L, Austin CP. DISC1 (Disrupted-In-Schizophrenia 1) is a centrosome-associated protein that interacts with MAP1A, MIPT3, ATF4/5 and NUDEL: regulation and loss of interaction with mutation. Hum Mol Genet. 2003;12:1591–608.
30. Soda T, et al. DISC1-ATF4 transcriptional repression complex: dual regulation of the cAMP-PDE4 cascade by DISC1. Mol Psychiatry. 2013;8:898–908.
31. Sawamura N, et al. Nuclear DISC1 regulates CRE-mediated gene transcription and sleep homeostasis in the fruit fly. Mol Psychiatry. 2008;13:1138–48. 1069
32. Malavasi EL, Ogawa F, Porteous DJ, Millar JK. DISC1 variants 37W and 607F disrupt its nuclear targeting and regulatory role in ATF4-mediated transcription. Hum Mol Genet. 2012;21:2779–92. https://doi.org/10.1093/hmg/dds106
33. Wen Z, et al. Synaptic dysregulation in a human iPS cell model of mental disorders. Nature. 2014;515:414–8. https://doi.org/10.1038/nature13716
34. Yoon KJ, et al. Modeling a genetic risk for schizophrenia in iPSCs and mice reveals neural stem cell deficits associated with adherens junctions and polarity. Cell Stem Cell. 2014;15:79–91. https://doi.org/10.1016/j.stem.2014.05.003
35. Kim D, et al. TopHat2: accurate alignment of transcriptomes in the presence of insertions, deletions and gene fusions. Genome Biol. 2013;14:R36. https://doi.org/10.1186/gb-2013-14-4-r36
36. Anders S, Pyl PT, Huber W. HTSeq–a Python framework to work with high-throughput sequencing data. Bioinformatics. 2015;31:166–9. https://doi.org/10.1093/bioinformatics/btu638
37. Love MI, Huber W, Anders S. Moderated estimation of fold change and dispersion for RNA-seq data with DESeq2. Genome Biol. 2014;15:550. https://doi.org/10.1186/s13059-014-0550-8
38. Huang da W, Sherman BT, Lempicki RA. Systematic and integrative analysis of large gene lists using DAVID bioinformatics resources. Nat Protoc. 2009;4:44–57. https://doi.org/10.1038/nprot.2008.211
39. Wang J, Duncan D, Shi Z, Zhang B. WEB-based GEne SeT anaLysis toolkit (WebGestalt): update 2013. Nucleic Acids Res. 2013;41:W77–83. https://doi.org/10.1093/nar/gkt439
40. Wickham H. ggplot2: elegant graphics for data analysis. New York: Springer-Verlag; 2016.
41. Zeng Y, et al. Lin28A binds active promoters and recruits Tet1 to regulate gene expression. Mol Cell. 2016;61:153–60. https://doi.org/10.1016/j.molcel.2015.11.020
42. Ho SY, et al. NeurphologyJ: an automatic neuronal morphology quantification method and its application in pharmacological discovery. BMC Bioinform. 2011;12:230. https://doi.org/10.1186/1471-2105-12-230
43. Shen Y, et al. TALOS+: a hybrid method for predicting protein backbone torsion angles from NMR chemical shifts. J Biomol NMR. 2009;44:213–23. https://doi.org/10.1007/s10858-009-9333-z
44. Brunger AT, et al. Crystallography & NMR System (CNS), A new software suite for macromolecular structure determination. Acta Crystallogr D. 1998;54:905–21. https://doi.org/10.1107/s0907444998003254
45. Koradi R, et al., MOLMOL: A program for display and analysis of macromolecular structures. J Mol Graphics. 1996;14:51–5.
46. Laskowski RA, et al. AQUA and PROCHECK-NMR: Programs for checking the quality of protein structures solved by NMR. J Biomol NMR. 1996;8:477. https://doi.org/10.1007/BF00228148
47. Chiang CH, et al. Integration-free induced pluripotent stem cells derived from schizophrenia patients with a DISC1 mutation. Mol Psychiatry. 2011;16:358–60. https://doi.org/10.1038/mp.2011.13
48. Sachs NA, et al. A frameshift mutation in disrupted in schizophrenia 1 in an American family with schizophrenia and schizoaffective disorder. Mol Psychiatry. 2005;10:758–64.
49. Chu CT, Plowey ED, Wang Y, Patel V, Jordan-Sciutto KL. Location, location, location: altered transcription factor trafficking in neurodegeneration. J Neuropathol Exp Neurol. 2007;66:873–83. https://doi.org/10.1097/nen.0b013e318156a3d7
50. Costa-Mattioli M, et al. eIF2alpha phosphorylation bidirectionally regulates the switch from short- to long-term synaptic plasticity and memory. Cell. 2007;129:195–206. https://doi.org/10.1016/j.cell.2007.01.050
51. Richter JD, Klann E. Making synaptic plasticity and memory last: mechanisms of translational regulation. Genes Dev. 2009;23:1–11.
52. St Clair D, et al. Association within a family of a balanced autosomal translocation with major mental illness. Lancet. 1990;336:13–16.
53. Genovese G, et al. Increased burden of ultra-rare protein-altering variants among 4,877 individuals with schizophrenia. Nat Neurosci. 2016;19:1433–41. https://doi.org/10.1038/nn.4402
54. Kano SI, et al. Host-parasite interaction associated with major mental illness. Mol Psychiatry. 2018. https://doi.org/10.1038/s41380-018-0217-z

Affiliations

Xinyuan Wang[1,2] · Fei Ye[3,4] · Zhexing Wen[5,6] · Ziyuan Guo[2] · Chuan Yu[3] · Wei-Kai Huang[2,7] · Francisca Rojas Ringeling[8] · Yijing Su[2] · Wei Zheng[9] · Guomin Zhou[1] · Kimberly M. Christian[2] · Hongjun Song[2,10,11,12] · Mingjie Zhang[3,4] · Guo-li Ming[2,10,11,13]

1 School of Basic Medical Sciences, Fudan University, 200032 Shanghai, China

2 Department of Neuroscience and Mahoney Institute for Neurosciences, Perelman School for Medicine, University of Pennsylvania, Philadelphia, PA 19104, USA

3 Division of Life Science, State Key Laboratory of Molecular Neuroscience, Hong Kong University of Science and Technology, Clear Water Bay, Kowloon, Hong Kong, China

4 Center of Systems Biology and Human Health, Hong Kong University of Science and Technology, Clear Water Bay, Kowloon, Hong Kong, China

5 Department of Psychiatry and Behavioral Sciences, Emory University School of Medicine, Atlanta, GA 30322, USA

6 Department of Cell Biology, Emory University School of Medicine, Atlanta, GA 30322, USA

7 Pathology Graduate Program, Johns Hopkins University School of Medicine, Baltimore, MD 21205, USA

8 The Human Genetics Pre-doctoral Program, Johns Hopkins University School of Medicine, Baltimore, MD 21205, USA

9 National Center for Advancing Translational Sciences, National Institutes of Health, Bethesda, MD 20892, USA

10 Department of Cell and Developmental Biology, Perelman School for Medicine, University of Pennsylvania, Philadelphia, PA 19104, USA

11 Institute for Regenerative Medicine, Perelman School for Medicine, University of Pennsylvania, Philadelphia, PA 19104, USA

12 The Epigenetics Institute, Perelman School for Medicine, University of Pennsylvania, Philadelphia, PA 19104, USA

13 Department of Psychiatry, Perelman School for Medicine, University of Pennsylvania, Philadelphia, PA 19104, USA